

Detailed studies of IPHAS sources - III. The highly extinguished bipolar planetary nebula IPHASX J191104.8+060845

J.B. Rodríguez-González^{1*}, L. Sabin², J.A. Toalá¹, S. Zavala³, G. Ramos-Larios⁴,
M.A. Guerrero⁵, Q.A. Parker^{6,7}, P.F. Guillén⁸ and A. Ritter⁶

¹*Instituto de Radioastronomía y Astrofísica (IRyA), UNAM Campus Morelia, Apartado postal 3-72, 58090 Morelia, Michoacan, Mexico*

²*Instituto de Astronomía, Universidad Nacional Autónoma de México, Apdo. Postal 877, 22800 Ensenada, B.C., Mexico*

³*Tecnológico Nacional de México / I. T. Ensenada (TecNM/ITE), Blvd. Tecnológico No. 150, C. P. 22780, Ensenada, B. C., Mexico*

⁴*Instituto de Astronomía y Meteorología, Universidad de Guadalajara, Av. Vallarta 2602, Arcos Vallarta, 44130 Guadalajara, Mexico*

⁵*Instituto de Astrofísica de Andalucía (IAA-CSIC), Glorieta de la Astronomía S/N, E-18008 Granada, Spain*

⁶*Physics Department, CYM Building, The University of Hong Kong, Pokfulam, Hong Kong SAR, China.*

⁷*Laboratory for Space Research, Hong Kong University, Hong Kong, China*

⁸*Instituto de Astronomía, Universidad Nacional Autónoma de México, Observatorio Astronómico Nacional, Ensenada, Baja California, Mexico*

24 September 2020

ABSTRACT

We present the first detailed study of the bipolar planetary nebula (PN) IPHASX J191104.8+060845 (PN G 040.6–01.5) discovered as part of the Isaac Newton Telescope Photometric H α Survey of the Northern Galactic plane (IPHAS). We present Nordic Optical Telescope (NOT) narrow-band images to unveil its true morphology. This PN consists of a main cavity with two newly uncovered extended low-surface brightness lobes located towards the NW and SE directions. Using near-IR *WISE* images we unveiled the presence of a barrel like structure, which surrounds the main cavity, which would explain the dark lane towards the equatorial regions. We also use Gran Telescopio de Canarias (GTC) spectra to study the physical properties of this PN. We emphasise the potential of old PNe detected in IPHAS to study the final stages of the evolution of the circumstellar medium around solar-like stars.

Key words: stars: evolution — stars: winds, outflows — planetary nebulae: general — planetary nebulae: individual: IPHASX J191104.8+060845

1 INTRODUCTION

Planetary nebulae (PNe) are the ejected remnants of the last evolutionary stages of low- and intermediate-mass stars ($M_{\text{ZAMS}} \lesssim 1-8 M_{\odot}$). During the asymptotic giant branch (AGB) phase, these stars lose mass through a slow ($v_{\text{AGB}} \approx 10-30 \text{ km s}^{-1}$) and dense ($\dot{M} \lesssim 10^{-5} M_{\odot} \text{ yr}^{-1}$) wind that produces shells that interact directly with the circumstellar medium (see [Tweedy & Kwitter 1994](#)). Stars in the AGB phase exhibit a relatively low effective temperature of $T_{\text{eff}} \approx 3,000-6,000 \text{ K}$ which allows the formation of dust shells ([Cox et al. 2012](#)). When the star finally expels its outer layers, a hot stellar core is exposed. These post-AGB stars can produce fast winds ($v_{\infty} = 500 - 4,000 \text{ km s}^{-1}$; [Guerrero, & De Marco 2013](#)) that will shock and compress the AGB material whilst it is being photoionised by the stellar raising UV flux. The combination of such effects produces a PN now emanating from the heating stellar core.

PNe are the outcome of the most numerous population of stars in the Universe (e.g. solar-like stars). In our Galaxy, the number of PNe has been estimated to range between 6,600 – 46,000 depending on the adopted scenarios and nebular sizes (e.g., [De Marco, & Moe 2005](#); [Frew, & Parker 2006](#); [Moe, & De Marco 2006](#); [Zijlstra,](#)

& [Pottasch 1991](#)). Around 3,500 PNe have been confirmed in our Galaxy thanks principally to the advent of wide field narrow band H α surveys of the Galactic Plane (e.g. [Parker et al. 2005](#); [Drew et al. 2005](#)) that permitted discovery of $\sim 2,000$ additional PNe (e.g. [Parker et al. 2006](#); [Miszalski et al. 2008](#); [Sabin et al. 2014](#)) and now increasingly thanks to the tireless work of the amateur community (e.g., [Kronberger et al. 2014](#)). A full PNe registry can be found in the Hong Kong/AAO/Strasbourg H α (HASH) PN database ([Parker, Bojičić & Frew 2016](#)). Increasing the number of known PNe is of importance to improve our understanding of the luminosity function of PNe, galactic chemical enrichment, stellar population synthesis, and galactic abundance gradients.

The Isaac Newton Telescope Photometric H α Survey of the Northern Galactic plane (IPHAS; [Drew et al. 2005](#); [González-Solares, et al. 2008](#); [Barentsen, et al. 2014](#)) has been designed to unveil the presence of mostly faint emission-line objects located in the Northern Galactic plane and hence characterised by higher extinction and by their advanced evolutionary phase or large distances ([Sabin et al. 2014](#)). IPHAS is a photometric CCD survey which covered the inner regions of the northern plane ($-5^{\circ} < b < 5^{\circ}$ and $29^{\circ} < l < 215^{\circ}$) with a total area coverage of 1800 deg^2 . The survey made use of the Wide Field Camera (WFC) on the Isaac Newton Telescope (INT) 2.5 m at La Palma in the Canary Islands (Spain) which has a field

* E-mail: j.rodrguez@irya.unam.mx

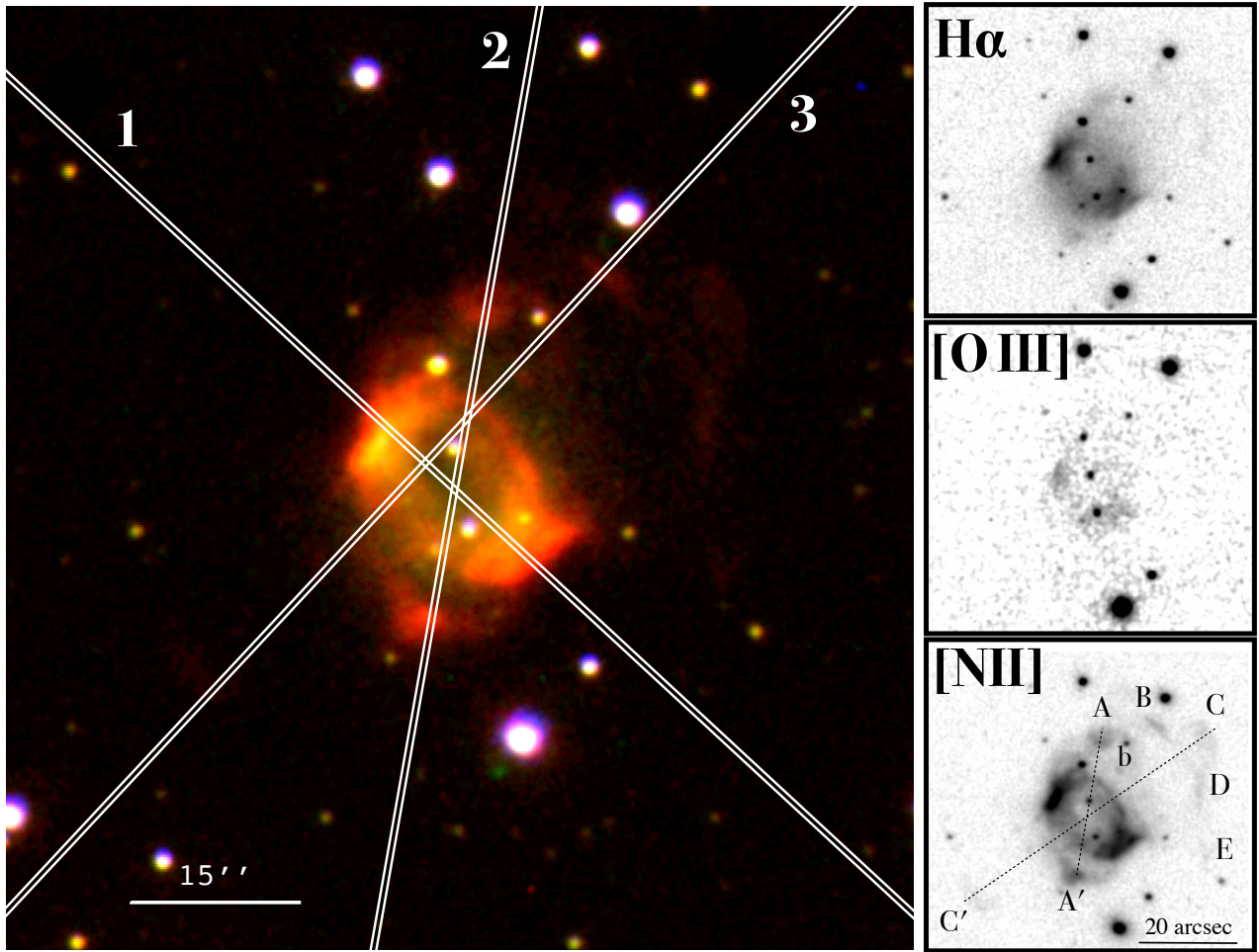


Figure 1. Colour-composite picture (left) and narrow band images (right) of IPHASX J191104.8+060845 obtained with the Nordic Optical Telescope. Red, green and blue correspond to [N II], H α and [O III], respectively. The position of the MES Echelle slits are labeled as 1, 2 and 3 and correspond to PA of +47°, −10° and −43°, respectively. The clumps around the main nebular shell are labeled in the [N II] image (lower right panel) referred in Section 3.2. The dotted lines connect the lobes of what we believe to be pairs of bipolar ejections. In all panels north is up, east to the left.

of view of $34 \times 34 \text{ arcmin}^2$ and a pixel scale of $0.33 \text{ arcsec pix}^{-1}$. The median seeing value was 1.1 arcsec. The good spatial resolution of the IPHAS data, as well as the use of binned mosaics (Sabin 2008), made this survey ideal for the detection of extended evolved PNe at the faint end of the PNe luminosity function. As a result, a total of 159 likely and possible PNe were confirmed with all types of morphologies (see Sabin et al. 2014). An additional sample of PNe will be presented soon (Ritter et al. in prep.). In order to confirm the PN nature of objects detected in IPHAS, a combination of different observational tools such as deep images and spectra is required (e.g., Frew & Parker 2010). This is the third paper of a series in which we characterise in detail interesting PNe from IPHAS (Sabin et al. 2020 and Guerrero et al 2020, both submitted to MNRAS). Here we present the analysis of the PN IPHASX J191104.8+060845 (a.k.a. PN G 040.6−01.5; hereafter J191104), confirmed spectroscopically on the GTC/OSIRIS (2018 May 17). We characterise its nature, morphology and physical properties. The paper is organized as follows. In Section 2 we present our observations, in Section 3 we present the analysis of our images and spectra and in Section 4 we discuss our results. Finally, the summary is presented in Section 5.

2 OBSERVATIONS

2.1 ALFOSC Optical Imaging

We observed J191104 with the Nordic Optical Telescope (NOT) at the Observatorio de El Roque de los Muchachos (ORM) in La Palma (Spain) with the Alhambra Faint Object Spectrograph and Camera (ALFOSC)¹ on 2018 June 14 using H α , [O III] and [N II] narrow-band filters. The central wavelength and FWHM are 6563 Å and 10 Å for H α , 5007 Å and 30 Å for [O III] and 6584 Å and 10 Å for [N II]. Bias and flat-field images were obtained to produce the final narrow-band filter images following standard procedures in IRAF (Tody 1993). Individual H α , [N II] and [O III] narrow-band filter images as well as a colour-composite image of J191104 are presented in Figure 1.

2.2 OSIRIS Long slit spectroscopy

Long slit intermediate resolution spectra were acquired with the Optical System for Imaging and low-Intermediate Resolution Integrated

¹ <http://www.not.iac.es/instruments/alfosc/>

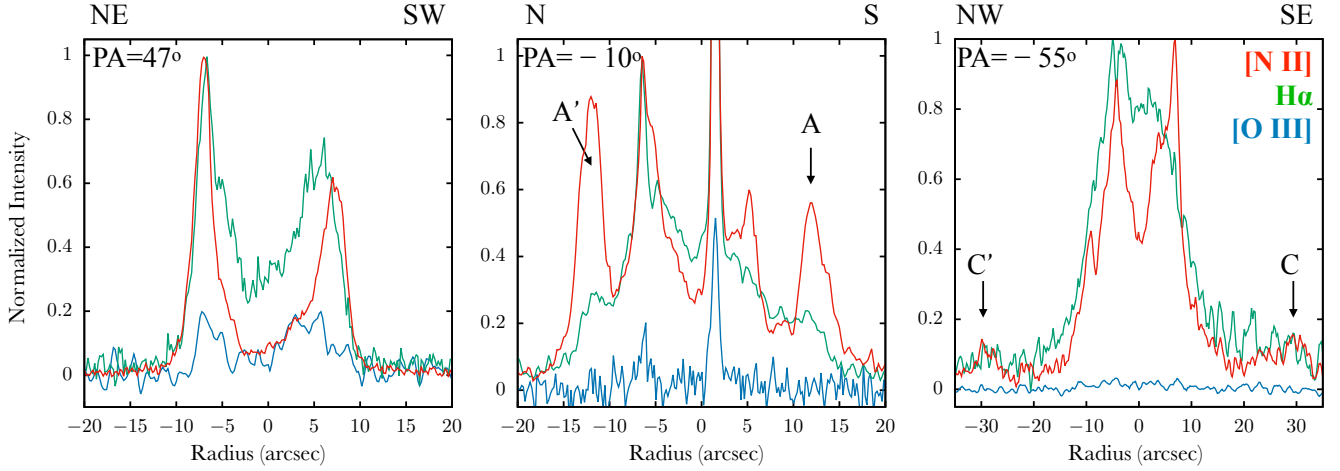


Figure 2. Normalised surface brightness profiles extracted from the NOT images. The left, center and right panels show the corresponding profiles extracted from PA= $+47^\circ$, -10° and -55° , respectively. The contribution from a star in the field of view of the three emission lines can be seen at $\sim 2''$ in the middle panel.

Spectroscopy instrument (OSIRIS; Cepa et al. 2003) mounted on the 10.4 m GTC telescope at the ORM. The observations were performed on 2018 May 17 using the two Marconi CCD42-82 (2048×4096) detectors with a 2×2 binning leading to a spatial scale of $0''.254 \text{ pix}^{-1}$. We used the R1000B grism covering a spectral range from 3630 \AA to 7500 \AA with a spectral dispersion of $2.12 \text{ \AA pix}^{-1}$. The slit width was set to $0.8''$ and the $7.4'$ length slit was placed at a position angle (PA) $+47^\circ$ through the main elongated bright structure. We obtained two spectra of 1000s exposure each. The HgAr and Ne lamps were used for wavelength calibration and the spectrophotometric standard star GD 140 for flux calibration. The observations were performed during dark time and clear sky but the seeing condition of $1.7''$ were not optimal. Data reduction was performed using standard IRAF routines.

2.3 MES long slit high resolution spectroscopy

We obtained long-slit high dispersion optical spectra of J191104 with the Manchester Echelle Spectrograph (MES; Meaburn et al. 2003) mounted on the 2.12 m telescope at the Observatorio Astronómico Nacional, San Pedro Mártir (OAN-SPM, Mexico). The data were obtained on 2018 July 22 and 2019 June 27 with a 2048×2048 pixels E2V CCD detector with pixel size of $13.5 \mu\text{m pixel}^{-1}$. MES has a fixed slit length of 6.5 and we set the slit width to $150 \mu\text{m}$ corresponding to $\sim 1''.9$. Two different pixel binning were used, 2×2 and 4×4 , leading to spatial scales of $0''.351 \text{ pixel}^{-1}$ and $0''.702 \text{ pixel}^{-1}$, respectively. The exposures times were 1200 s and 1800 s and three spectra were taken with the $\text{H}\alpha$ filter with $\Delta\lambda = 90 \text{ \AA}$ to isolate the 87th order (0.05 and $0.1 \text{ \AA pixel}^{-1}$ spectral scale for the 2×2 binning and 4×4 binning, respectively). The slits were arranged at PAs $+47^\circ$, -10° , -43° in order to cover the main morphological structures of the target. The slit positions are shown in Figure 1 and labeled as Slit 1, 2 and 3, respectively. The spectral range includes the $\text{H}\alpha$ and $[\text{N II}] \lambda\lambda 6548, 6584 \text{ \AA}$ emission lines.

3 RESULTS

3.1 Morphology

The NOT images presented in Figure 1 show that J191104 is a nebula with a clear bipolar morphology. We thus re-classify the morphology as Bspam following the adopted HASH scheme (see Parker et al. 2006). Its main nebular shell exhibits a bright ellipse detected in $[\text{N II}]$ with lesser contribution from $\text{H}\alpha$ and marginally detected in $[\text{O III}]$. This structure appears brighter at the south-west and north-east and is $18'' \times 12''$ in size. Assuming that it corresponds to a projected circular ring, we estimate that it is tilted 42° with respect to the plane of the sky.

A collection of knots detected in the $[\text{N II}]$ image can be seen towards the north-west from the central ring. These have been labeled from A to E (see lower-right panel of Fig. 1). Only two of these seem to have counterparts towards the south-east from the central ring. We have labeled these as A' and C'. The pairs A–A' and C–C', connected with dashed-lines in the bottom-right panel of Figure 1, are equidistant from the center of the ring at $\sim 14''$ and $\sim 30''$. The pair A–A' is also detected in the $\text{H}\alpha$ narrow-band image but the position of the other knots is only suggested in this image. None of these structures are detected in the $[\text{O III}]$ image.

In order to peer further into the structure of J191104, we have extracted surface brightness profiles from the three nebular images. We have selected PAs of $+47^\circ$, -10° and -55° to extract 1D profiles from the three narrow-band filter images. These three PAs trace the surface brightness distribution of the central ring, the direction of the A–A' knots and that of the C–C' knots, respectively. All profiles are presented in Figure 2. This figure shows that the $[\text{N II}]$ emission encloses that of $\text{H}\alpha$ and $[\text{O III}]$. The elliptical structure is illustrated by the leftmost panel of Figure 2. The profiles of the three emission lines show that the south-west region of the ellipse is broader than the north-east region with FWHM of $\sim 5''$ for the $[\text{N II}]$ emission profile.

The middle panel of Figure 2 shows that the A–A' pair of knots are broad and comparable to that of the main elliptical shell profile. They exhibit a FWHM of $\sim 4 - 5''$. This pair of knots is also marginally detected in the $\text{H}\alpha$ emission profile (see Fig. 1). Figure 2 also shows that the A–A' pair of knots are as bright as the elliptical main shell in

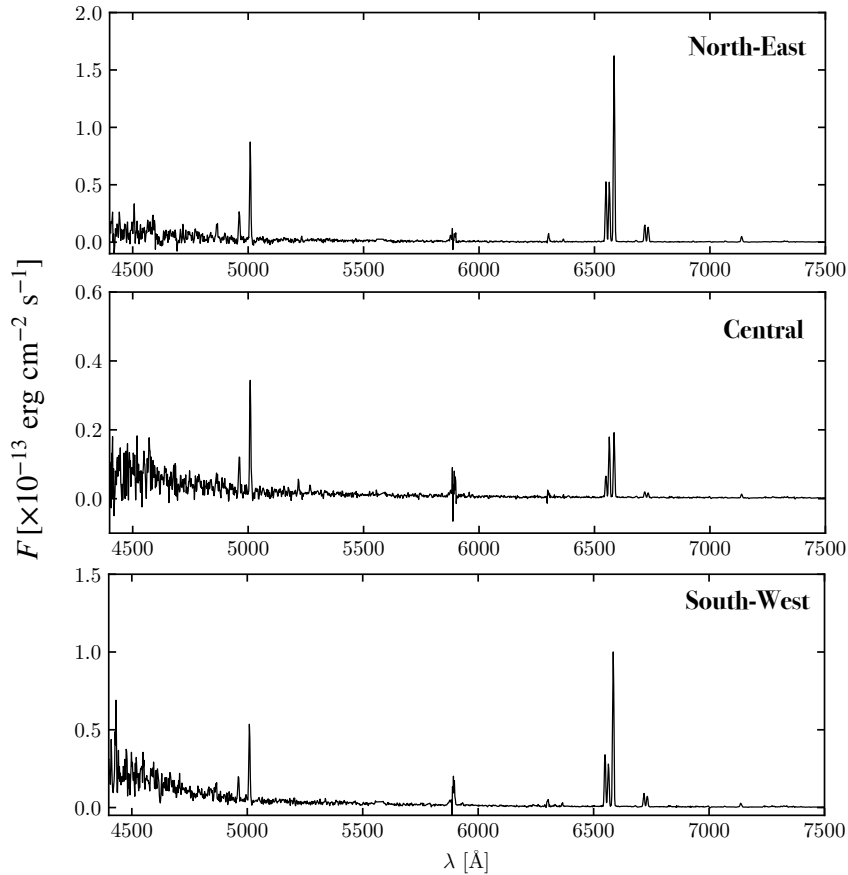


Figure 3. GTC OSIRIS dereddened spectra of IPHASX J191104.8+060845. The upper, middle and bottom panels show the spectra of the North-East, central and South-west region of the main ellipsoidal structure.

J191104. On the other hand, the rightmost panel of Figure 2 shows that the C–C′ pair is dimmer. Finally, we note that the middle and right panels of Figure 2 also show that the H α exhibit a center-filled morphology filling the inner [N II] shell.

3.2 Chemistry

We extracted three spectra from the GTC spectrum, two corresponding to the bright rims of the central ring denoted as North-East (NE) and South-West (SW) and another from the central region of the main cavity in J191104. These are shown in Figure 3. According to the images presented in Figure 1, the spectra are dominated by the [N II] line at 6584 Å. The contribution from other emission lines is smaller (see Fig. 3). All detected emission lines in the spectra are listed in Table 1.

Due to the similarity between the North-East and South-West spectra, we only present the analysis of the former. The spectrum is the one used to analyse the physical and chemical properties of J191104. The analysis tool ANNEB (Olguín et al. 2011), based on the *Nebular/IRAF* package (Shaw, & Dufour 1995), was used to derive the parameters of the nebula (this includes using the atomic data from IRAF libraries). The logarithmic extinction i derived from H α /H β Balmer decrement is found to be particularly high, with $c(\text{H}\beta) = 3.36 \pm 0.16$. This corresponds to a reddening $E(B - V) = 2.77 \pm 0.13$ in concordance with the extinction values in this line of sight given in

the Galactic DUST Reddening and Extinction² at the NASA/IPAC Infrared Science Archive. The dereddening of the emission lines was performed using the extinction curve from Fitzpatrick, & Massa (2007) for $R_V = 3.1$. Details of the line fluxes are listed in Table 1.

The logarithmic flux ratios shown in Table 2 are used to position our target in updated diagnostic diagrams by Frew & Parker (2010) and Sabin et al. (2013), and confirm the PN nature of J191104.8, though morphology alone in these new deeper narrow-band images are already highly indicative. The source is characterised by a low electronic temperature, $T_e(\text{[N II]}) = 8000 \pm 1800$ K, and a low density of $N_e = 260 \pm 20 \text{ cm}^{-3}$ as estimated from the [S II] $\lambda\lambda 6717, 6731$ doublet. We note that our density estimate is at the edge of the physical lower limit derived by this method (Osterbrock & Ferland 2006). J191104 has too few lines to perform a detailed abundance analysis, but we were able to obtain some mean ionic abundances for the North-East spectrum. These are listed in Table 3. Due to the low ionization state of the nebula we do not expect species with very high ionization degree. Based on the ionic abundances results and assuming that these can be approximated to the total abundances (e.g. $\text{N}^+/\text{O}^+ \sim \text{N}/\text{O}$) it appears that J191104.8 is rich in He, O and N.

Based on the spectroscopic analysis we are able to assert the PN nature of J191104. Unfortunately, due to the low emission we cannot derive the total abundances, but we can use the spectra and ionic abundances (using H^+) to classify this PN. To do so, we consider

² <https://irsa.ipac.caltech.edu/applications/DUST/>

Table 1. Emission lines detected in the GTC OSIRIS North-East spectrum of J191104.8+060845[†].

Ion	λ_0	F	F^*
H β [†]	4861	100 ± 24	100 ± 24
[O III]	4959	208 ± 38	173 ± 32
[O III]	5007	735 ± 126	559 ± 97
[N II]	5755	26 ± 30	6 ± 7
He I	5876	157 ± 37	28 ± 8
[O I]	6300	333 ± 60	34 ± 9
[O I]	6363	110 ± 24	10 ± 3
[N II]	6548	3,833 ± 655	287 ± 85
H α	6563	3,883 ± 663	286 ± 55
[N II]	6583	12,300 ± 2,100	885 ± 263
He I	6678	107 ± 28	7 ± 3
[S II]	6716	1,307 ± 224	81 ± 25
[S II]	6731	1,221 ± 209	74 ± 23
He I	7065	102 ± 24	4 ± 2
[Ar III]	7136	652 ± 112	26 ± 9
[O II]	7320	136 ± 26	5 ± 2
[O II]	7330	81 ± 21	3 ± 1

*Dereddened values.

[†] All values are normalized to $F(\text{H}\beta)=100$ with $F_{\text{H}\beta} = (4.39 \pm 0.75) \times 10^{-17}$

Table 2. Flux ratios for the diagnostic diagrams

Species	Value	Error
$\log(\text{H}\alpha/[\text{N II}])$	-0.6	0.1
$\log(\text{H}\alpha/[\text{S II}])$	0.3	0.1
$\log([\text{O III}]/\text{H}\alpha)$	0.4	0.1
$[\text{S II}] 6716/6731$	1.2	0.3

the logarithmic flux ratios shown in Table 2 to position our target in diagnostic diagrams. J191104 falls in the region of Type I PNe (Peimbert 1978; Peimbert & Serrano 1980). These objects are characterized by their enrichment in nitrogen and helium, with abundance ratios $\text{He}/\text{H} \geq 0.14$ and $\log(\text{N}/\text{O}) \geq -0.3$. It is believed that the excess in N and He abundance is the result of the evolution of progenitors more massive than $2.4 M_{\odot}$, which implies that it was recently formed from a medium that is presumably richer in metals and helium (Peimbert & Torres-Peimbert 1987). Furthermore, these nebulae have many filamentary structures and usually show a bipolar morphology. We found that J191104 has $\log(\text{N}/\text{O}) = 0.74 \pm 0.14$ and according to Peimbert's criterion, this PN agrees with a Type I PN.

3.3 Kinematics

The position-velocity (PV) diagrams obtained from our SPM-MES observations are shown in Figure 4. The top panels present the H α emission line extracted from the three slit positions shown in Figure 1, while the bottom panels of this figure present the corresponding [N II] emission line profiles. We first notice that the [N II] profiles clearly trace well-defined structures, whilst the H α profiles are fuzzy, thus in the following we describe the kinematics of J191104 only taking into account the [N II] line profiles.

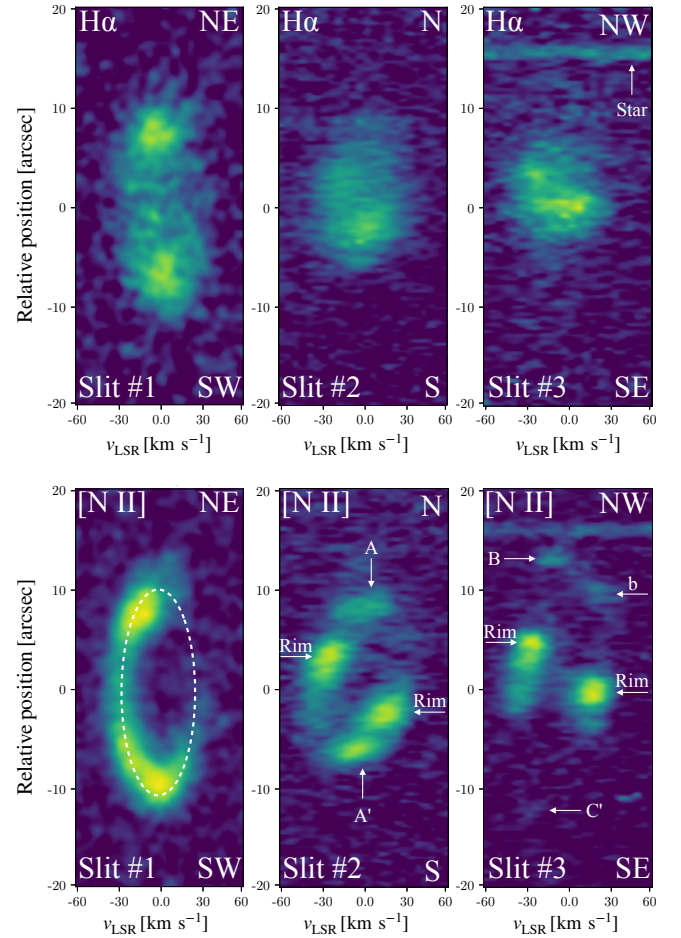
The Slit 1, which was obtained with a PA=47°, unveils the kinematics of the main cavity of J191104. This profile discloses the kinematic signature of an expanding ellipsoidal structure (Fig. 4 bottom left panel). The line profile lacks emission in the red shifted part

Table 3. Mean ionic abundances obtained from the GTC OSIRIS North-East spectrum of J191104.8+060845.

Ion	$N_{\text{ion}}/N_{\text{H}+}$	error (%) [*]	λ (Å) [†]
He ⁺	0.2	17.0	5876,6678,7065
N ⁺	2.0×10^{-4}	15.2	5755,6548,8583
S ⁺	2.0×10^{-6}	10.0	6716,6731
O ²⁺	2.0×10^{-4}	14.0	4959,5007
O ⁺	3.0×10^{-5}	109.0	7320,7330
Ar ²⁺	5.00×10^{-6}	22.5	7136

*The uncertainties in the ionic abundances are the result of propagating the line fluxes errors and those of electron temperature into the estimations.

[†] Wavelength of the emission lines used to compute the ionic abundance.


Figure 4. Echelle spectra obtained with the MES at SPM. From left to right, Slit #1, #2 and #3. The upper panels show the H α emission line and the bottom their corresponding [N II] emission. Note the contribution from a background star in the Slit #3 spectra.

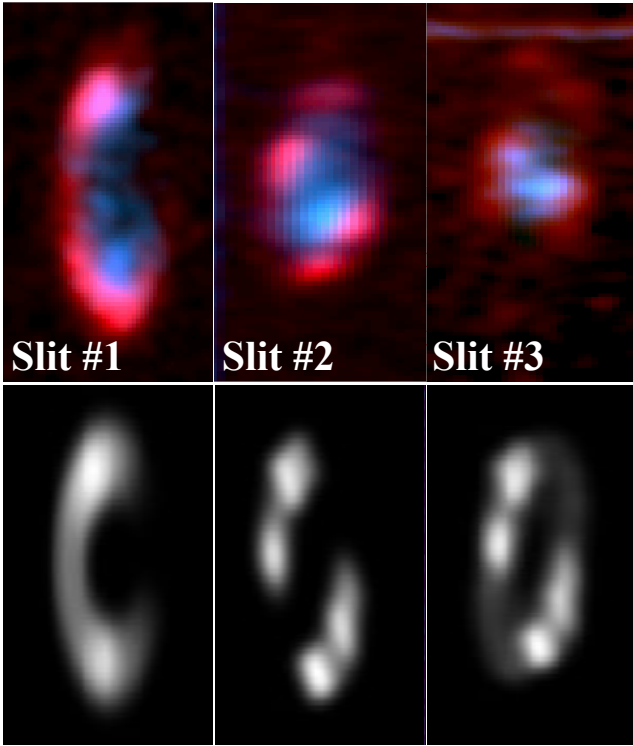


Figure 5. Colour-composite images of the PV shown in Fig. 4. In the top panel, red and blue correspond to the emission from [N II] and H α , respectively. The bottom panels show the synthetic PV images from our best SHAPE morphokinematic model obtained in section 4.2

of the spectrum. The expansion velocity obtained by fitting an ellipse to the line profile (see Fig. 4 bottom left panel) is 26 km s^{-1} .

Slits 2 and 3 trace the velocity components of the central ring-like structure and are labeled accordingly in Figure 4. They also exhibit some structures, which extend NW–SE according to the nebular images presented in Figure 1. The Slit 2 (PA= -10°), which covers the positions of the A–A’ pair of knots, shows that the brightest region of these features have velocities close to zero, although they extend from $\sim 20 \text{ km s}^{-1}$ to $\sim -27 \text{ km s}^{-1}$ with respect to the systemic velocity of the main shell.

Slit 3 (PA= -43°) covers the positions of the features labeled as B, b and C’. The bottom right panel of Figure 4 suggests that the knots B and b are part of a lobe that expands towards the NW protruding from the inner ring. Their velocity difference is $\sim 60 \text{ km s}^{-1}$. The C’ knot is marginally detected in the panel at a velocity of -28 km s^{-1} . The expansion velocity of the ring obtained from Slits 2 and 3 are 23.5 km s^{-1} and 23 km s^{-1} , respectively, which are consistent with that estimated from Slit 1.

In Figure 5 we present colour-composite images combining the spectra presented in Figure 4. This figure shows that although the structures are not traced in detail by the H α profiles, the H α emission is contained inside the [N II] emission. Gas that emits in this line has thus lower expansion velocities than that of the [N II]-emitting gas.

4 DISCUSSION

The images and spectra presented in the previous sections show that J191104 is a PN with low-ionization structures. Its emission is

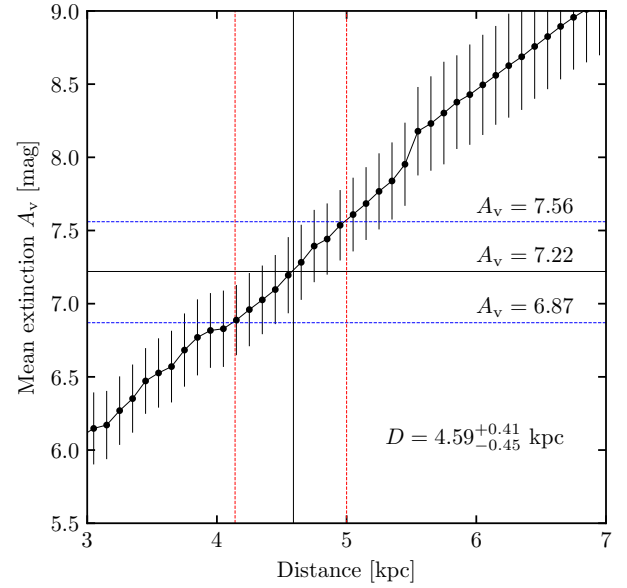


Figure 6. Estimated distance as a function of mean extinction A_v following the method described by Sale et al. (2014).

dominated by the [N II] line and the PN shows a small contribution from the [O III] line. In order to unveil its origin we have performed several analysis to try to assess the characteristics of this PN and its central star.

4.1 Physical properties and structure of J191104

To determine the physical size of J191104 we need to estimate the distance to this PN. It is impossible to determine the distance using the central star because, as we show in the following section, identifying the progenitor star is a difficult task. Thus, we need to use indirect methods such as the one proposed by Frew, Parker & Bojicic (2016). These authors developed a statistical method to calculate distances to PNe using the H α surface brightness ($S_{H\alpha}$). This quantity can be defined as

$$S_{H\alpha} = \frac{F_{H\alpha}}{A}, \quad (1)$$

Where A represents the angular area of the object in steradians (sr) and $F_{H\alpha}$ is the flux of the object in the H α emission line in units of $\text{erg cm}^{-2} \text{ s}^{-1}$. Thus, we need to estimate the total H α luminosity and surface brightness of J191104. For this we used our GTC OSIRIS spectra of the central region of J191104. The H α flux was scaled to an ellipsoidal region with semi-axis of $11'' \times 8''$, which encompasses the main cavity in J191104. We found an H α surface brightness of $S_{H\alpha} = 2.84 \times 10^{-5} \text{ erg cm}^{-2} \text{ s}^{-1} \text{ sr}^{-1}$.

Frew, Parker & Bojicic (2016) presented different relationships between $S_{H\alpha}$ and the size (r) according to the characteristics of the PN. One of the criteria to determine the type of nebula is the flux ratio between the [N II] 6584 Å and H α emission lines. If $F(\text{[N II] } 6584\text{Å})/F(\text{H}\alpha) \geq 1$ we are in the optically thick regime for PNe. This is the case for our PN where we find a ratio of 3.3. The corresponding $S_{H\alpha} - r$ relation for this type of nebula is:

$$\log S_{H\alpha} = -(3.32 \pm 0.12) \log r - (4.97 \pm 0.08). \quad (2)$$

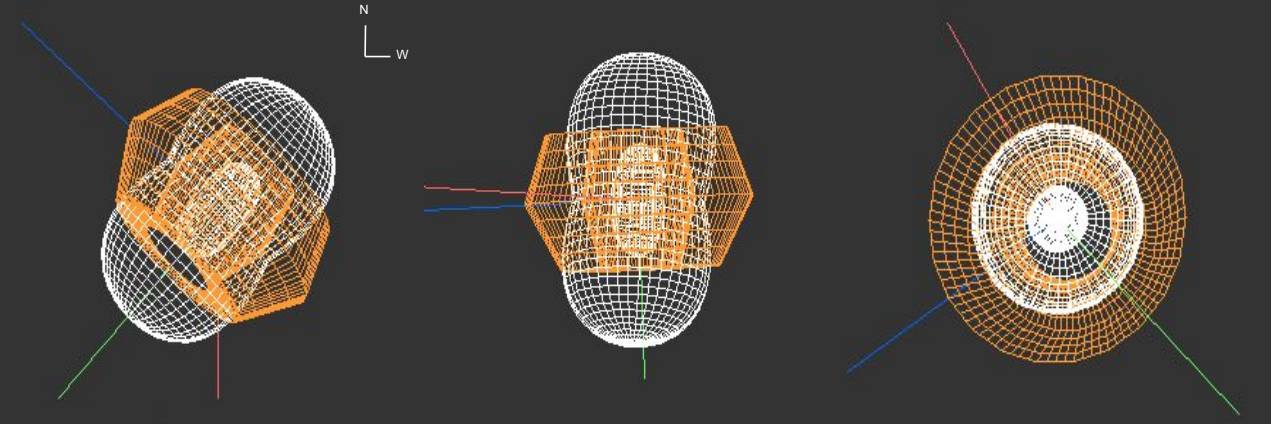


Figure 7. Morpho-kinematic SHAPE model of IPHASX J191104.8+060845 based on PV diagrams presented in Figure 4. The left panel corresponds to the nebula projected onto the plane of the sky, in the central panel we have a side view and in the right panel a view through the lobe.

Using our estimate of the $S_{H\alpha}$ we obtained $r = 0.75 \pm 0.04$ pc. Then, the distance can be calculated as

$$D \approx 206265 \left(\frac{r}{\text{pc}} \right) \left(\frac{\theta}{''} \right)^{-1} \text{ pc}, \quad (3)$$

where θ is in this case the largest extension of J191104, using scale plate we find $\theta = 30''$. By adopting this value for θ we are assuming the somewhat evident fact that the $H\alpha$ emission from the central region of J191104 dominates the total $H\alpha$ flux. Then, the distance to J191104 is $D = 5.1 \pm 0.3$ kpc.

Another way of determining the distance is calculating the extinction towards stars in the vicinity of J191104 following the method described by Sale et al. (2014). This is based on the relationship between the extinction of a source and that of field's stars in the IPHAS sky with known distances located in the source line of sight. The extinction map is illustrated in Figure 6 and we used $A_V = 2.15 \times c(H\beta)$ for coherence with the maps generation method. The resulting distance is $D_2 = 4.6^{+0.4}_{-0.5}$ kpc which is consistent with that derived following above.

Using the two independent distance estimates we can calculate an averaged distance of $D = 4.9 \pm 0.6$ kpc and we can now proceed to calculate a dynamical age for the morphological components in J191104. The inner ring has an extension of 0.26 pc and using our MES observations we found that the main cavity is expanding with a velocity of 23 ± 3 km s⁻¹. Thus a kinematical age, τ can be obtained as:

$$\tau \approx 978000 \left(\frac{r}{\text{pc}} \right) \left(\frac{v}{\text{km/s}} \right)^{-1}. \quad (4)$$

We find that J191104 has a kinematic age $\tau = 11,000 \pm 1,500$ yr.

4.2 Morpho-kinematics Modelling

In order to interpret the MES observations and to unveil the kinematic structure of J191104 we have used SHAPE (Steffen et al. 2011). SHAPE is used to reconstruct and model the morpho-kinematic signatures of astrophysical objects. Using this software we can build a morpho-kinematic model that reproduces the PV diagrams in Figure 4. Our best model was achieved by a main barrel-like structure with an inclination of 42° , which corresponds to the central part of the nebula showing the highest emission. It is also necessary to add a hollow bipolar structure with a similar inclination. In Figure 7 we present

the visualization of our SHAPE model with different perspectives. Synthetic spectra obtained from similar positions as those shown in Figure 1 are compared to the MES observations in Figure 5. We note that the observations obtained from slit 3 might suggest that the NW lobe has sub-structures (see Fig. 4 and 5). This might be the same case for the SE lobe, but self absorption due to dust in this PN (see next section) hampers a stronger statement. Furthermore, a better representation of the observations is severely hampered by the fact that the faint structures are below detection limits of MES.

4.3 Searching for a progenitor

Identifying the progenitor star of J191104 is not a trivial task. One might have expected that as a first approximation the progenitor star should be projected (or contained) within the inner cavity of J191104. There are two apparent stars that come close to this condition (see Fig. 1). However, these two sources are located close to the rim of the inner cavity making them unlikely to be the progenitor star.

As a first step to try to identify the progenitor star of J191104 we searched the UV-Excess survey (UVEX; Groot et al. 2009)³. This is a complementary survey to the IPHAS which maps the Northern Galactic Plane ($b < 5^\circ$) with the 2.5 m INT but with the U , g , r , and $\text{He I } 5875$ filters. UVEX looks for hot, blue objects, with relatively low luminosity. However, looking at the UVEX survey data, we could not find any noticeable central star. Also PanSTARRS (Chambers, et al. 2016) g band shows no signs of detection either. Based on the weakest field star in PanSTARRS, we establish that the central star will have a magnitude dimmer than 21. This tells us that the central star must be an evolved low luminosity object that might also be obscured by dust in the nebula.

Furthermore, we also searched the IR catalogues at IRSA⁴ for obscured candidates. The 2MASS images of the vicinity of J191104 revealed the presence of point-like sources which are coincident with those detected in optical images (see Fig. 8). A search in the WISE data of the vicinity of J191104 show no apparent correlation with point sources but extended mid-IR emission. The WISE W3 at $12 \mu\text{m}$ and W4 at $22 \mu\text{m}$ images exhibit a single maximum associated with the inner region of the main cavity. If one takes into account the morpho-kinematic model presented in the previous section (see the

³ <https://www.astro.ru.nl/uvex/Science.html>

⁴ <https://irsa.ipac.caltech.edu/frontpage/>

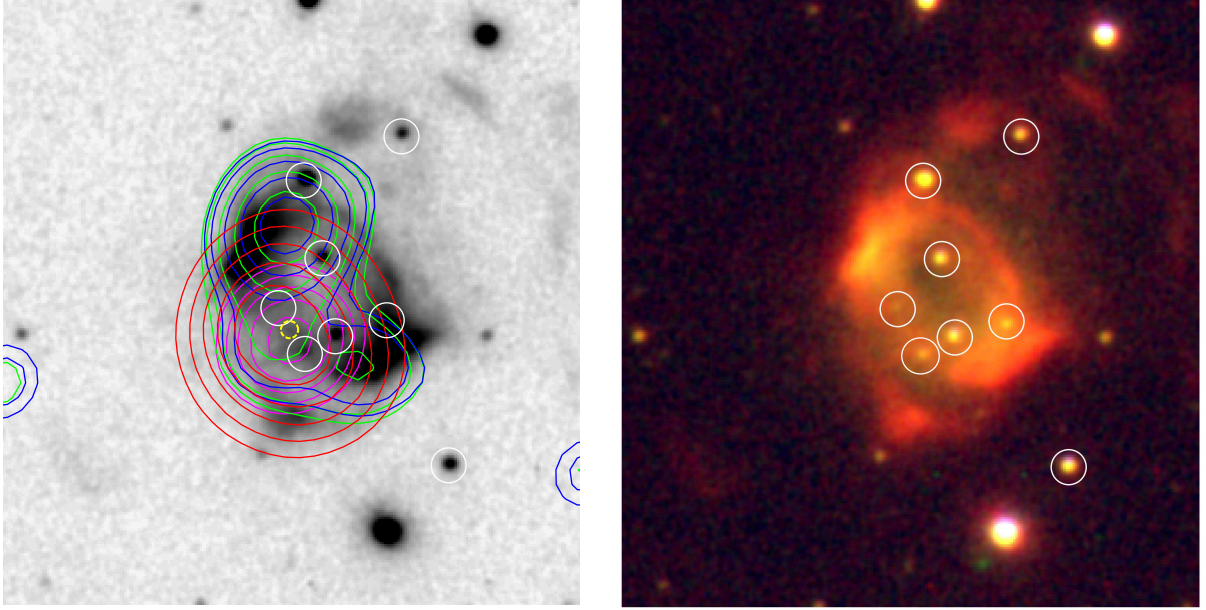


Figure 8. Comparison between IR and optical emission from IPHASX J191104.8+060845. Left: Grey-scale [N II] image. The magenta, red, green and blue contours correspond to the near-IR emission detected by *WISE* bands W4 22 μm , W3 12 μm , W2 4.6 μm , and W1 3.4 μm , respectively. Right: Colour-composite optical image similar to Figure 1. The white circles show the positions of stars detected in the optical and 2MASS images. North is up, East to the left.

innermost structure in the right panel of 7), we can suggest a position for the central star, and thus assume that it is placed close to the geometric center of the nebula (i.e. slightly off centered). This is also illustrated with a yellow dashed-line circle in the left panel of Figure 8. This position seems to be coincident with the *WISE* W3 and W4 bands maxima which might point at the location of the progenitor star of J191104, although the resolution is not sufficient to strongly constrain this suggestion.

On the other hand, the *WISE* W1 at 3.4 μm and W2 at 4.6 μm bands exhibit morphologies very similar as those traced by the [N II] NOT image (Figure 8). Two near-IR maxima are associated to the NE and SW edges of the inner cavity of J191104. For comparison we show in the left panel of Figure 8 the [N II] emission compared with contours obtained from the four *WISE* bands. Figure 8 points at the presence of dust associated to the main cavity structure in J191104 which might be responsible for extinguishing the brightness of the SE lobe.

Here we have shown that J191104 is an old, evolved, heavily reddened and extinguished PNe. The present work suggests that dust has survived the evolution of the CSPN for 11,000 yr. This means that the barrel-like structure might have been dense enough to shield dust from the UV flux. Another possibility is that dust has recently formed due to the reduction of the ionizing photon flux from the progenitor star. This is an interesting idea worth pursuing with the characterization of IPHAS objects. The very late stages of evolution of PNe have not been studied in detail. For example, what are the observable properties of PNe in which the power of the stellar wind has diminished (e.g., [García-Segura et al. 2006](#)).

5 CONCLUSION

We have presented a multi-frequency study of the nebula IPHASX J191104.8+060845 (J191104) originally detected in the IPHAS. We

have used images and spectra to demonstrate that this is in fact a bipolar, heavily-extincted, old PN. Our findings can be summarized as:

- Using GTC OSIRIS spectra we found that the $\log(\text{N/O})$ ratio is 0.74 ± 0.14 and $\text{He/H} \gg 0.20$. Thus it can be classified as a Peimbert Type I, which means that J191104 has been formed by the evolution of a massive progenitor star very likely more massive than $2.4 M_{\odot}$. The electron density and temperature are found to be $N_e = 200 \pm 20 \text{ cm}^{-3}$ and $T_e = 8000 \pm 1800 \text{ K}$.
- Our NOT images unveiled the presence of a bright central elliptical structure surrounded by detached patches of emission mostly detected in [N II] and marginally in the $H\alpha$ image. Some of the clumps seem to be paired and are located towards the NW and SE from the main inner cavity. Faint extended bipolar lobes are also revealed for the first time.
- Using two independent methods we estimate that the distance to J191104 is $D \approx 4.9 \text{ kpc}$ and with the help of the MES observations we calculated a kinematical age of 11,000 yr.
- The kinematic data obtained from our MES observations help us reconstruct, as a first approximation, the structure and kinematics of J191104. For this, we used the interactive 3D morpho-kinematic application SHAPE. Our best model of J191104 suggests that the PN is composed by a main barrel-like dense structure with a hollow, bipolar structure. The morphology of the structures towards the NW of the main cavity suggests that several lobes might exist in J191104. The high extinction revealed by the optical and IR images might hamper the detection of the SE lobes
- We did not identify a progenitor star using the UVEX catalogue, but the analysis of IR observations agree with the suggested position for the progenitor star (assuming that it should be located at the geometric center of J191104). Furthermore, the IR observations suggest that the dust is spatially correlated with the main cavity in J191104. Either dust has survived the evolution of the central star for the past

11,000 yr or it has recently formed due to the reduction of the UV flux of the progenitor star.

IPHAS is giving us the unique possibility of studying old and/or extinguished objects in the North Galactic plane. Although much attention has been paid to aspherical, young PNe with the *Hubble Space Telescope* (see Hsia et al. 2014; Sahai et al. 2011, and references therein) this is the missing link to study the fate of the circumstellar matter around solar-like stars. We will be able to study phases in which the stellar wind dims and the UV flux practically disappears leaving the ionized gas to evolve under its own inertia. These evolved PNe will also allow us to assess whether dust survives the evolution of the PNe or if dust is being formed due to the reduction of the UV flux from the CSPN.

ACKNOWLEDGEMENTS

The authors are thankful to the referee for a prompt report that improved the presentation of the present paper. J.B.J.-G. and J.A.T. are funded by UNAM DGAPA PAPIIT projects IA100318 and IA100720. J.B.J.-G. and L.S. are funded by UNAM-PAPIIT grant IN101819. SZ works under the collaboration agreement "UNAM-TecNM 43310-3020-30-IX-15". GR-L acknowledges support from CONACyT and PRODEP (México). MAG acknowledges support from the Spanish Government Ministerio de Ciencia, Innovación y Universidades through grant PGC2018-102184-B-I00. QAP thanks the Hong Kong Research Grants Council for GRF research support under grants 17326116 and 17300417. We thank the daytime and night support staff at the OAN-SPM for facilitating and helping obtain our observations. This paper makes use of data obtained as part of the INT Photometric $H\alpha$ Survey of the Northern Galactic Plane (IPHAS) carried out at the Isaac Newton Telescope (INT). The INT is operated on the island of La Palma by the Isaac Newton Group in the Spanish Observatorio del Roque de los Muchachos of the Instituto de Astrofísica de Canarias. All IPHAS data are processed by the Cambridge Astronomical Survey Unit, at the Institute of Astronomy in Cambridge. Based on observations collected at the Observatorio Astronómico Nacional at San Pedro Mártir, B.C., Mexico. Based on observations made with the Nordic Optical Telescope, operated by the Nordic Optical Telescope Scientific Association at the Observatorio del Roque de los Muchachos, La Palma, Spain, of the Instituto de Astrofísica de Canarias. Based on observations made with the Gran Telescopio Canarias (GTC), installed at the Spanish Observatorio del Roque de los Muchachos of the Instituto de Astrofísica de Canarias, in the island of La Palma. The data presented here were obtained in part with ALFOSC, which is provided by the Instituto de Astrofísica de Andalucía (IAA) under a joint agreement with the University of Copenhagen and NOTSA.

DATA AVAILABILITY

The data underlying this article will be shared on reasonable request to the corresponding author.

REFERENCES

Barentsen G., et al., 2014, MNRAS, 444, 3230
 Cepa, J., Aguiar-Gonzalez, M., Bland-Hawthorn, J., et al. 2003, Proc. SPIE, 4841, 1739
 Chambers K. C., et al., 2016, arXiv, arXiv:1612.05560

Cox, N. L. J., Kerschbaum, F., van Marle, A.-J., et al. 2012, A&A, 537, A35.
 De Marco, O., & Moe, M. 2005, Planetary Nebulae as Astronomical Tools, 169.
 Drew J. E., et al., 2005, MNRAS, 362, 753
 Fitzpatrick, E. L., & Massa, D. 2007, ApJ, 663, 320
 Frew, D. J., Parker, Q. A., & Bojičić, I. S. 2016, MNRAS, 455, 1459
 Frew, D. J., & Parker, Q. A. 2006, Planetary Nebulae in Our Galaxy and Beyond, 49
 Frew D. J., Parker Q. A., 2010, PASA, 27, 129
 García-Segura, G., López, J. A., Steffen, W., et al. 2006, ApJ, 646, L61
 González-Solares E. A., et al., 2008, MNRAS, 388, 89
 Groot, P. J., Verbeek, K., Greimel, R., et al. 2009, MNRAS, 399, 323
 Guerrero, M. A., & De Marco, O. 2013, A&A, 553, A126.
 Hsia, C.-H., Chau, W., Zhang, Y., et al. 2014, ApJ, 787, 25
 Kronberger, M., Jacoby, G. H., Acker, A., et al. 2014, Asymmetrical Planetary Nebulae VI Conference, 48.
 Meaburn, J., López, J. A., Gutiérrez, L., et al. 2003, Rev. Mex. Astron. Astrofis., 39, 185
 Miszalski, B., Parker, Q. A., Acker, A., et al. 2008, MNRAS, 384, 525.
 Moe, M., & De Marco, O. 2006, ApJ, 650, 916.
 Olguín, L., Vázquez, R., Contreras, M. E., et al. 2011, Revista Mexicana De Astronomia Y Astrofisica Conference Series, 193
 Osterbrock, D. E. & Ferland, G. J. 2006, Astrophysics of gaseous nebulae and active galactic nuclei, 2nd. ed. by D.E. Osterbrock and G.J. Ferland. Sausalito, CA: University Science Books, 2006
 Parker Q. A., et al. 2005, MNRAS, 362, 689
 Parker, Q. A., Acker, A., Frew, D. J., et al. 2006, MNRAS, 373, 45
 Parker Q. A., Bojičić I. S., Frew D. J., 2016, JPhCS, 32008, JPhCS.728
 Peimbert, M. 1978, Planetary Nebulae, 215
 Peimbert, M., & Serrano, A. 1980, Rev. Mex. Astron. Astrofis., 5, 9
 Peimbert, M., & Torres-Peimbert, S. 1987, Rev. Mex. Astron. Astrofis., 14, 540
 Sabin L., 2008, PhD
 Sabin, L., Parker, Q. A., Corradi, R. L. M., et al. 2014, MNRAS, 443, 3388.
 Sabin, L., Parker, Q. A., Contreras, M. E., et al. 2013, MNRAS, 431, 279
 Sahai, R., Morris, M. R., & Villar, G. G. 2011, AJ, 141, 134
 Sale, S. E., Drew, J. E., Barentsen, G., et al. 2014, MNRAS, 443, 2907
 Shaw, R. A., & Dufour, R. J. 1995, PASP, 107, 896
 Steffen, W., Koning, N., Wenger, S., et al. 2011, IEEE Transactions on Visualization and Computer Graphics, 17, 454
 Tody, D. 1993, Astronomical Data Analysis Software and Systems II, 173
 Tweedy, R. W & Kwitter, K. B. 1994, AJ, 108, 1
 Zijlstra, A. A., & Pottasch, S. R. 1991, A&A, 243, 478.